Formation and Reactions of the Heme−Dioxygen Intermediate in the First and Second Steps of Nitric Oxide Synthesis As Studied by Stopped-Flow Spectroscopy under Single-Turnover Conditions†

Susan Boggs,‡ Liuxin Huang,‡ and Dennis J. Stuehr*

Department of Immunology, Lerner Research Institute, Cleveland Clinic, Cleveland, Ohio 44195

Received August 27, 1999; Revised Manuscript Received December 13, 1999

ABSTRACT: To better understand the mechanism of nitric oxide (NO) synthesis, we studied conversion of *N*-hydroxy-L-arginine (NOHA) or L-arginine (Arg) to citrulline and NO under single-turnover conditions using the oxygenase domain of neuronal nitric oxide synthase (nNOSoxy) and rapid scanning stopped-flow spectroscopy. When anaerobic nNOSoxy saturated with H_4B and NOHA was provided with 0.5 or 1 electron per heme and then exposed to air at 25 °C, it formed 0.5 or 1 mol of citrulline/mol of heme, respectively, indicating that NOHA conversion had 1:1 stoichiometry with respect to electrons added. Identical experiments with Arg produced substoichiometric amounts of NOHA or citrulline even when up to 3 electrons were provided per heme. Transient spectral intermediates were investigated at 10 °C. For NOHA, four species were observed in the following sequence: starting ferrous nNOSoxy, a transient ferrous−dioxygen complex, a transient ferric−NO complex, and ferric nNOSoxy. For Arg, transient intermediates other than the ferrous−dioxygen species were not apparent during the reaction. Our results provide a kinetic framework for formation and reactions of the ferrous−dioxygen complex in each step of NO synthesis and establish that (1) the ferrous−dioxy enzyme reacts quantitatively with NOHA but not with Arg and (2) its reaction with NOHA forms 1 NO/heme, which immediately binds to form a ferric heme−NO complex.

The nitric oxide synthases (NOSs)[1] catalyze a stepwise oxidation of L-arginine (Arg) to nitric oxide (NO) and citrulline (*1*−*3*). Three mammalian NOS have been cloned from a variety of sources. Each consists of an N-terminal oxygenase domain that binds iron protoporphyrin IX (heme), 6-(*R*)-tetrahydrobiopterin (H_4B), and Arg and a C-terminal reductase domain that binds FMN, FAD, and NADPH, with a ∼20 amino acid calmodulin binding motif located between the two domains (*4*, *5*). To be active, two NOS polypeptides must form a homodimer. The interaction primarily occurs between two oxygenase domains (*6*) and forms an extensive dimer interface (*7*−*9*). The fact that NOS oxygenase domains can fold and function properly when expressed independent of their reductase domains has facilitated spectroscopic, mutagenic, and crystallographic studies of this domain (*7*−*17*).

The NO synthesis reaction is complex and not completely understood. Stoichiometric, stable isotope, spectroscopic, and crystallographic studies are consistent with a heme-based mechanism shown in Figure 1 (*1*−*3*). In the first step, Arg is hydroxylated to the intermediate N^{ω}-hydroxy-L-arginine (NOHA), and 1 mol of NADPH and O_2 are consumed. In the second step NOHA is oxidized to citrulline and NO, with consumption of 0.5 mol of NADPH and 1 mol of O_2. Oxygen activation in both steps is carried out by the enzyme-bound heme, which derives electrons from NADPH via the flavin-containing reductase domain and possibly from H_4B.

One unusual feature of the proposed mechanism is that distinct heme−oxy species may participate in each step of the reaction (Figure 1). For example, in the first step the ferrous−dioxygen species ($Fe^{II}O_2$) is thought to only be an intermediate on the path to the ultimate oxidant (a heme oxo−iron species, FeO),[2] whereas in the second step the $Fe^{II}O_2$ species could react directly with NOHA. Overall, the two-step mechanism in Figure 1 is consistent with spectral evidence of O_2 binding to the heme iron (*18*−*21*), a close proximity between bound Arg and the heme (*7*−*9*, *17*), a high reactivity for the NOHA guanidino carbon toward hydroxide or peracid nucleophiles (*22*), and no net donation of electrons from H_4B.

The mechanism in Figure 1 predicts that furnishing a single electron and O_2 to the heme should enable NOS to convert one molecule of NOHA to citrulline and NO. This was first tested with full-length ferrous nNOS (*23*). In that study,

† This work was supported by National Institutes of Health Grant GM51491 to D.J.S. and a Fellowship Award from Berlex Biosciences to L.H. This work was presented in abstract form at the 1998 meeting of the American Society of Biochemistry and Molecular Biology in Washington, DC.

* Corresponding author: Immunology NB-3, Lerner Research Institute, Cleveland Clinic, 9500 Euclid Ave., Cleveland, OH 44195. Phone 216-445-6950; FAX 216-444-9329; E.mail stuehrd@ccf.org.

‡ These authors contributed equally.

[1] Abbreviations: Arg, L-arginine; H_4B, (6*R*)-2-amino-4-hydroxy-6-(L-*erythro*-1,2-dihydroxypropyl)-5,6,7,8-tetrahydropteridine; nNOS, neuronal nitric oxide synthase; nNOSoxy, the oxygenase domain of neuronal nitric oxide synthase; NOHA, N^{ω}-hydroxy-L-arginine.

[2] This species is more formally represented as $(Fe^{IV}{=}O)^{2+}$, with a cation radical present on the porphyrin, a protein residue, or H_4B. It is designated FeO for simplicity.

10.1021/bi9920228 CCC: $19.00
Published on Web 02/10/2000

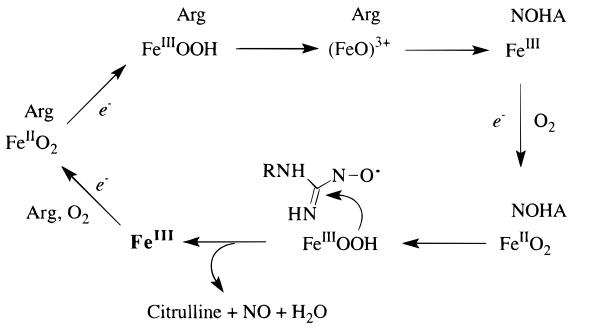

FIGURE 1: Proposed mechanism of NO synthesis by NOS. Provision of Arg, an electron from the reductase domain, and O_2 to H_4B-saturated ferric NOS (bold Fe^{III}) forms a substrate-bound, transient $Fe^{II}O_2$ complex. Provision of a second electron forms a transient $Fe^{III}OOH$ species that undergoes oxygen−oxygen bond scission to lose water and form the electrophilic oxo−iron species $(FeO)^{3+}$, which hydroxylates Arg to form enzyme-bound NOHA and ferric NOS. Provision of O_2 and an electron from the reductase domain regenerates the $Fe^{II}O_2$ complex, which then obtains a second electron to generate a NOHA radical and the nucleophilic $Fe^{III}OOH$ species. These react as shown by the curved arrow to form a species that electronically rearranges to form products and ferric enzyme. Adapted from refs *1*−*3* and *25*.

citrulline was formed in a 1:1 ratio with respect to nNOS, along with a substoichiometric amount of nitrite. Although NO formation was not directly demonstrated, this result did suggest that a reaction may occur between NOHA and the $Fe^{II}O_2$ species in the second step that is sufficient to drive the reaction to completion. When Arg was substituted for NOHA in the same study, no products (NOHA, citrulline, or nitrite) were detected, consistent with the first step of NO synthesis requiring that two electrons be provided to the heme to generate the FeO species before a reaction with Arg can occur.

A subsequent study with ferrous nNOS or its oxygenase domain essentially confirmed the NOHA results, but in addition reported that as much as 0.5 mol of Arg/mol of nNOS could be converted to NOHA in the same system (*19*). In addition, spectral data collected in the presence of Arg at −30 °C (*19*, *21*) suggested that heme−oxy species could form whose spectra were distinct from those previously reported for the nNOS $Fe^{II}O_2$ species in aqueous buffer at 10 °C (*18*, *20*). Together, this led one group to suggest that bound H_4B might provide an electron to the $Fe^{II}O_2$ species for Arg hydroxylation in their system (*19*). Indeed, a recent report shows that an H_4B radical can form in this setting when Arg is bound (*35*). Thus, fundamental questions remain regarding the spectral properties and reactivity of the $Fe^{II}O_2$ species in each step of NO synthesis, electron donation from H_4B, and the exact nature of the nitrogen oxide product that is formed with citrulline.

To address these issues, we combined stoichiometric analysis with stopped-flow kinetic methods to investigate formation and reactivity of the $Fe^{II}O_2$ species in each step of NO synthesis. We used the oxygenase domain of nNOS (nNOSoxy) and dithionite as electron donor in place of full-length nNOS and NADPH because nNOSoxy is available in sufficient quantity for single-turnover studies and contains no reductase domain flavins to complicate interpretation of the spectra. Our results (1) provide a kinetic framework that links $Fe^{II}O_2$ formation with product formation in a single-turnover setting, (2) help clarify if H_4B serves as an electron donor, and (3) establish that NO is an immediate reaction product of NOHA oxidation.

MATERIALS AND METHODS

Materials and Enzyme Purification. NOHA was purchased from Alexis. All other materials were obtained from sources reported previously (*18*, *23*, *28*). Rat nNOSoxy (amino acids 1−720) containing a six-histidine tag at the C terminus was overexpressed in *Escherichia coli* and purified in the absence of Arg and H_4B as described previously (*18*). Enzyme concentration was determined from the 444 nm absorbance of the ferrous−CO complex by using an extinction coefficient of 76 mM^{-1} cm^{-1}.

Preparation of Reaction Solution and Samples. A 0.7 mL solution of ferric nNOSoxy (20 μM) containing 100 μM H_4B, 1 mM DTT, and 0.1 mM NOHA (or Arg) in 40 mM Hepes, pH 7.5, was placed in an anaerobic cuvette and made anaerobic by alternately evacuating and flushing with oxygen-free argon at 25 °C (*18*). In some cases, catalase (100 units/mL) and superoxide dismutase (10 units/mL) were also added to the reaction. The enzyme was then reduced by titrating with a dithionite solution of known concentration in a gastight syringe. The absorption spectrum of the nNOSoxy solution was recorded with a Hitachi 3110 spectrophotometer after each addition of dithionite solution until the desired concentration of ferrous nNOSoxy was reached. Reactions were initiated by exposing the cuvette solutions to air. The solutions were filtered through Amicon Centricon concentrators (10 000 MW cutoff) and the filtrates were stored at −70 °C.

Measurement of NOHA and Citrulline. NOHA and citrulline in the reaction filtrates were measured by an HPLC method as described previously (*23*). Briefly, a portion of each filtrate was incubated with *o*-phthaldialdehyde reagent [0.1 M sodium borate containing 35 mM *o*-phthaldialdehyde, 10% (v/v) methanol, and 1% (v/v) mercaptoethanol] for 2 min and then injected onto a Hewlett-Packard ODS−Hypersil, 5 μm particle size, 2.1 × 100 mm reverse-phase HPLC column. The column was eluted at a flow rate of 0.75 mL/min with linear gradients of buffers A and B [buffer A, 5% CH_3CN, 0.1% (v/v) trifluoroacetic acid, and 15 mM sodium borate, pH 9.5; buffer B, 50% CH_3CN, 0.1% (v/v) trifluoroacetic acid, and 8 mM sodium borate, pH 9.5]. Derivatized NOHA and citrulline were detected by use of a flow-through Hitachi F-2000 fluorescence spectrophotometer set at 360 nm excitation and 455 nm emission and quantitated relative to NOHA and citrulline standards.

Nitrite Measurement. Nitrite was measured by the Griess assay in a 96-well microplate (*23*). Samples (0.1 mL) of the filtrate were mixed with 0.1 mL of Griess reagent in each well. The absorbance difference between 550 and 650 nm was read in a Thermomax microplate reader after 15 min, and nitrite was quantitated relative to sodium nitrite standards.

Stopped-Flow Experiments. Rapid-scan stopped-flow experiments were done on a stopped-flow apparatus from Hi-Tech Ltd. (model SF-51) equipped for anaerobic work and a Hi-tech MG-6000 rapid-scan diode-array detector. Anaerobic solutions of nNOSoxy containing 50 mM Hepes, pH 7.5, 0.2 mM H_4B, 1 mM DTT, and 0.2 mM NOHA, Arg, or no substrate were titrated spectrophotometrically with a dithion-

ite solution as described above until full reduction to ferrous nNOSoxy was achieved. The ferrous nNOSoxy solution was then transferred to the stopped-flow instrument, where it was rapidly mixed in multiple shots with an equal volume of air-saturated buffer (50 mM Hepes, pH 7.5) at 10 °C. Ninety-six spectral scans (350−700 nm) were obtained following each mixing. The diode-array data were then fit to different reaction models by a Specfit program from Hi-tech Ltd. to obtain the calculated number of species, their individual spectra, the concentration of each species versus time, and rate constants for each transition. The stopped-flow experiments were repeated with two or three different batches of nNOSoxy for each experimental condition.

RESULTS AND DISCUSSION

Conversion of NOHA to Citrulline and Nitrite under Single-Turnover Conditions. We had previously shown that providing a single electron to the heme of full-length nNOS allowed 1 mol of enzyme to catalyze the conversion of 1 mol of NOHA to citrulline plus nitrite (*23*). We therefore determined if our recombinant nNOSoxy would also catalyze conversion of NOHA to citrulline and nitrite under single-turnover conditions. Solutions of nNOSoxy containing NOHA and H_4B were reduced with 0.5, 1, or 2 equiv of dithionite/mol of heme under anaerobic conditions and then exposed to air to initiate the reaction.

When 17 μM heme protein was reduced with dithionite to the level of 1 electron equiv/mol of heme, 17 μM citrulline (Figure 2A) and 6.4 μM nitrite (Figure 2B) were produced from NOHA. When the enzyme was provided with 2 electron equiv/mol of heme, 18 μM citrulline and 8.2 μM nitrite was produced. Because the amounts of citrulline and nitrite were almost the same when 1 or 2 electron equiv were provided to each heme, this indicates that ferrous nNOSoxy reacted only once with O_2 and NOHA even in the presence of excess dithionite. It thus appears that excess dithionite was scavenged by solution O_2 before it could rereduce ferric nNOSoxy after the single turnover. When nNOSoxy was reduced with only 0.5 equiv of dithionite/mol of heme, 9 μM citrulline (Figure 2A) and 3.5 μM nitrite (Figure 2B) were formed, indicating a one-to-one relationship exists between the amount of citrulline formed and the initial amount of ferrous nNOSoxy. Inclusion of superoxide dismutase and catalase in the reaction did not lower product formation (data not shown). Control experiments run without dithionite generated no citrulline or nitrite from NOHA, and dithionite did not convert NOHA to products without enzyme (data not shown). Our results show that ferrous nNOSoxy catalyzed a quantitative conversion of NOHA and O_2 to citrulline in the single-turnover setting and thus support a mechanism where the $Fe^{II}O_2$ species is a competent reactant in the second step of NO synthesis.

Spectroscopy and Kinetics of Ferrous nNOSoxy Reaction with Oxygen and NOHA. To directly examine formation and reactivity of the $Fe^{II}O_2$ species in the second step, we utilized rapid-scanning stopped-flow spectroscopy to identify consecutive heme protein transitions that occur during conversion of NOHA to citrulline and nitrite. A solution of dithionite-reduced nNOSoxy saturated with H_4B and NOHA was rapid-mixed with air-saturated buffer at 10 °C. Ninety-six spectra were then recorded within 0.429 s, 12 of which

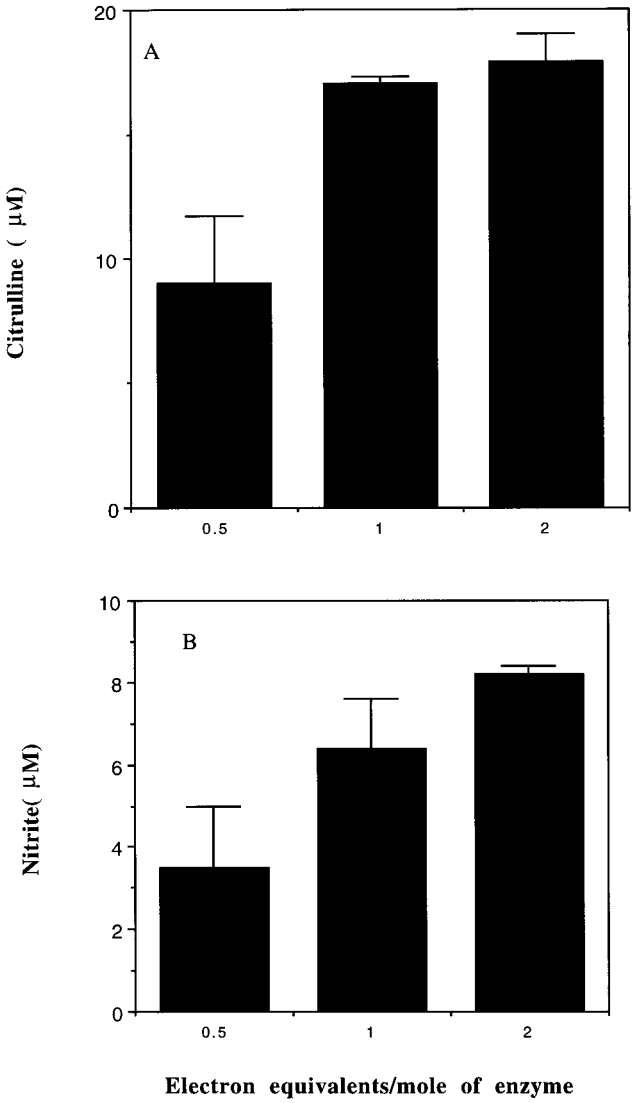

FIGURE 2: Conversion of NOHA to citrulline and nitrite by nNOSoxy in a single-turnover reaction. Anaerobic, H_4B- and NOHA-saturated nNOSoxy (17 μM) was reduced with dithionite to the levels indicated and then exposed to air. Citrulline formed in the reactions is shown in panel A, and nitrite formed is shown in panel B. Each bar represents the mean ± SD of two independent experiments, each assayed in triplicate.

are shown in Figure 3A. The rapid-scan data were best fit to a reaction model A to B to C to D by a Specfit program provided by the instrument manufacturer. The calculated spectra for species A−D are shown in Figure 3B. Species A has absorbance maxima at 416 and 557 nm, identifying it as the initial ferrous nNOSoxy species (*10, 18, 23*). Species B has absorbance maxima at 429 and 557 nm, consistent with the reported spectrum for the nNOS $Fe^{II}O_2$ complex at 10 °C in the presence of H_4B and substrate (*18, 20*). Species C has absorbance maxima at 440, 547, and 580 nm, identical to the spectrum of the ferric−NO complex of nNOS (*24*). Species D has absorbance maxima at 396 and 630 nm, identifying it as ferric nNOSoxy (*10, 18*). The time courses of spectral change recorded for eight experiments were each fit to the sum of three exponentials and gave three rate constants with values of 113 ± 20, 26 ± 2, and 5.4 ± 0.4 s^{-1} for the A to B, B to C, and C to D transitions, respectively. Figure 3C shows the calculated variation of concentration for species A−D over the course of the

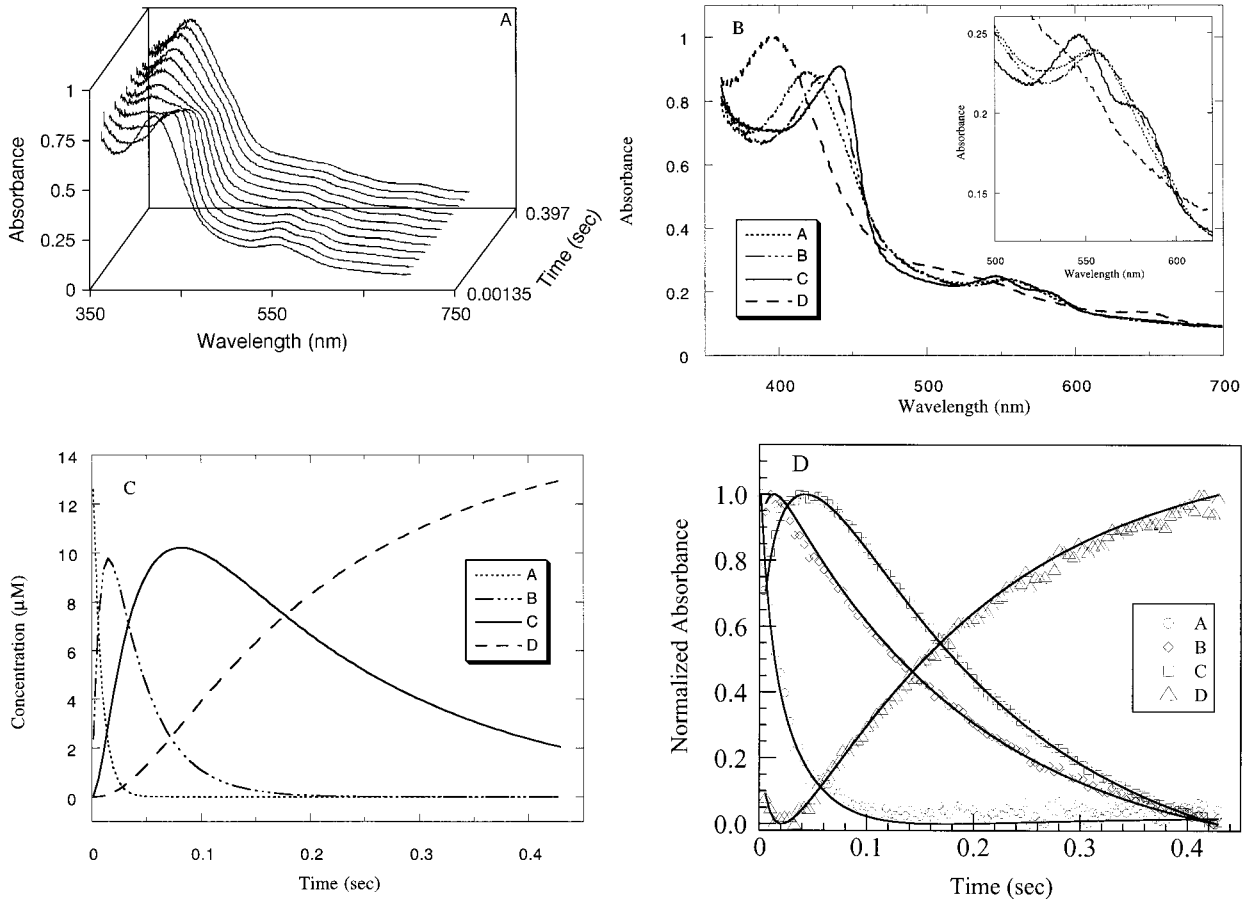

FIGURE 3: Rapid-scan stopped-flow analysis of the reaction of ferrous nNOSoxy with O_2 and NOHA. Ferrous nNOSoxy (30 μM) saturated with H_4B and NOHA was rapidly mixed with air-saturated buffer at 10 °C. Panel A shows 12 of the 96 consecutive spectra recorded within the first 0.429 s. Panel B shows the Specfit calculated spectra of four distinct species observed during the reaction. Species A, B, C, and D are the ferrous, $Fe^{II}O_2$, $Fe^{III}NO$, and ferric nNOSoxy, respectively. The inset expands the same spectral traces in the range of 500 and 620 nm. Panel C contains calculated plots of concentration of species A−D versus time. Panel D compares normalized absorbance values versus time for each species obtained from the data (symbols) with simulated absorbance versus time curves that were calculated using the kinetic model (—). Representative wavelengths were chosen at or near the absorbance maximum of each species.

reaction, while Figure 3D compares the actual change in absorbance attributed to each species with its calculated change in absorbance. These combined spectral and kinetic results provide compelling evidence for formation of the $Fe^{II}O_2$ complex and its quantitative reaction with NOHA in the second step of NO synthesis, and with the stoichiometry of product formation establish a kinetic mechanism for the second step shown in Scheme 1. Ferrous nNOSoxy binds O_2 in the initial step to generate the $Fe^{II}O_2$ complex, which reacts quantitatively with bound NOHA to generate NO and citrulline. NO then binds to form a ferric heme−NO complex, which decays to generate ferric nNOSoxy.

Scheme 1

$$Fe^{II} \xrightarrow{113\ s^{-1}} Fe^{II}O_2 \xrightarrow{26\ s^{-1}} Fe^{III}NO \xrightarrow{5\ s^{-1}} Fe^{III}$$

In Scheme 1, conversion of the $Fe^{II}O_2$ species to the ferric−NO complex actually represents the time frame where NO synthesis from NOHA took place during the single turnover at 10 °C. What exactly happens during this time period is still unclear. Conceivably, the $Fe^{II}O_2$ species could directly react with NOHA, followed by electron rearrangements to generate ferric enzyme, citrulline, NO, and water. However, no products are formed from NOHA during single turnover when the $Fe^{II}O_2$ intermediate is generated in the absence of H_4B (*19*, *23*). An alternative mechanism is shown in Figure 1 and has the $Fe^{II}O_2$ species reduced by a second electron to form a heme iron−peroxy species ($Fe^{III}OOH$), which undergoes nucleophilic reaction with the NOHA radical to form products. Conversion of NOHA to citrulline by both organic− and heme−peroxy nucleophiles is well-established (*22*, *38*). The second electron could be furnished either by NOHA (*1*−*3*, *25*) or by bound H_4B. However, if H_4B is the source of the second electron, then NOHA (or a later reaction intermediate) would have to reduce the pterin radical to regenerate H_4B, because NOHA must undergo a net three-electron oxidation to form NO (*1*−*4*).

The spectra of thiol-ligated $Fe^{II}O_2$ and $Fe^{III}OOH$ heme proteins are expected to differ (*26*). We therefore examined spectral traces recorded during formation of the $Fe^{II}O_2$ complex and its transition to the NO complex to check for evidence of $Fe^{III}OOH$ formation. Figures 4 and 5 contain spectral traces collected during formation of the $Fe^{II}O_2$ species and its subsequent reaction with NOHA to form the NO complex, respectively. Both transitions displayed isosbestic points (see arrows in figures) and were essentially monophasic when examined at single wavelengths (not shown). This indicates that no other spectrally distinct species

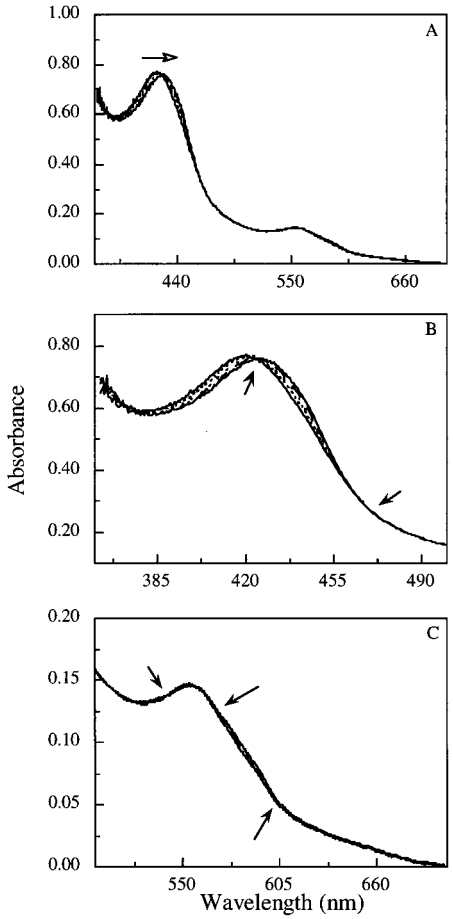

FIGURE 4: Overlay of spectral traces collected during formation of the $Fe^{II}O_2$ complex with NOHA. The four spectra were recorded within the time period of 0−8.8 ms. The open arrow shows the shift in Soret absorbance with time, while the solid arrows indicate isosbestic points. (A) Wavelength range from 360 to 700 nm; (B) expanded region 360−500 nm; (C) expanded region 500−700 nm.

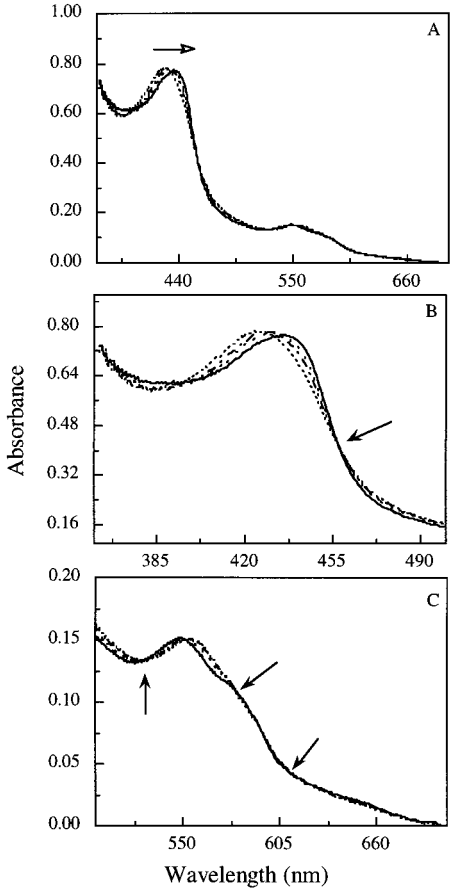

FIGURE 5: Overlay of spectral traces collected during conversion of the NOHA-saturated $Fe^{II}O_2$ complex to the ferric−NO complex. The four spectra shown were recorded within the time period of 7.4−37.4 ms. The open arrow shows the shift in Soret absorbance with time, while the solid arrows indicate isosbestic points. (A) Wavelength range from 360 to 700 nm; (B) expanded region 360−500 nm; (C) expanded region 500−700 nm.

built up during either transition, consistent with our Specfit analysis that showed only two transient intermediates. Thus, the $Fe^{III}OOH$ species either does not form during NO synthesis from NOHA, reacts more quickly than it forms, or has an absorption spectrum that cannot be distinguished from the $Fe^{II}O_2$ species under our experimental conditions.

The buildup of a ferric−NO species during NOHA oxidation in the single-turnover reaction has important implications regarding the reaction mechanism and regulation of NO synthesis. For example, the fact that the NO complex was ferric rather than ferrous establishes that nNOSoxy produced the NO radical as a primary product, rather than other *N*-oxides such as nitroxyl, which would generate a ferrous−NO complex with the heme. This in turn confirms that NOHA provides an electron to NOS for a net three-electron oxidation in the second step. The NOHA electron is provided either to the heme sometime after $Fe^{II}O_2$ complex formation or to the pterin radical as discussed above.

The kinetics of heme−NO complex formation and decay are such that up to 70% of the nNOSoxy molecules accumulated as a ferric−NO complex during the single-turnover reaction. This implies that each nNOSoxy heme bound the NO molecule that it made and could even indicate that a heme−NO bond forms as an integral step of NO synthesis. Such high trapping efficiency is consistent with stopped-flow and flash photolysis studies that show NO binds quickly to the ferric or ferrous heme of NOS, sometimes before it leaves the active site (*27*−*29*). Indeed, a similar degree of NO trapping probably occurs during steady-state NO synthesis by full-length nNOS, where between 70% and 90% of the enzyme molecules partition into a ferrous NO complex within the first few catalytic turnovers (*30*). In our current experiments, the decay rate of the ferric−NO complex probably reflects NO dissociation from ferric NOS, which is quite rapid (*27*−*29*). During NO synthesis by nNOS, our results suggest that NO initially binds to the ferric heme, followed by reduction to generate the ferrous−NO species that accumulates during the steady state.

There has been some discrepancy in the literature regarding the spectral properties of the nNOS $Fe^{II}O_2$ complex. Our spectral kinetic analysis of O_2 binding and subsequent reaction, with isosbestic points appearing as described, establishes that the species with 427 nm Soret absorbance is the $Fe^{II}O_2$ complex of nNOSoxy formed in the presence of substrate, as originally published by us (*18*) and for full-length nNOS by Sato et al. (*20*). This differs from the 415−419 nm $Fe^{II}O_2$ complex observed for nNOS at −30 °C by Bec et al. (*19*) and recently by Ledbetter et al. (*21*). Although a Soret absorbance around 416−418 nm is more typical for

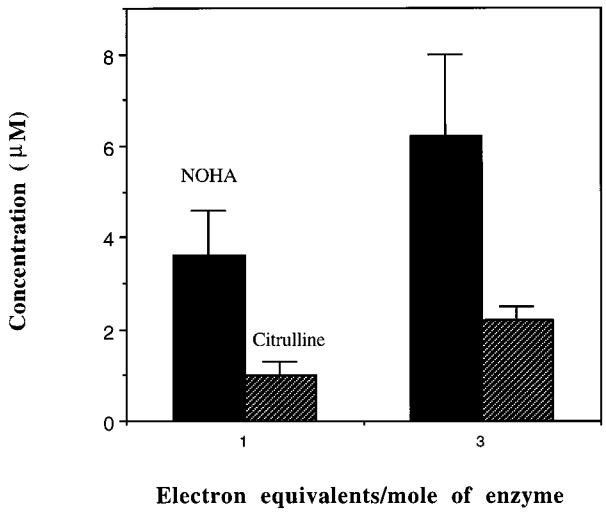

FIGURE 6: Conversion of Arg to NOHA and citrulline by nNOSoxy in a single-turnover reaction. Anaerobic, H_4B- and Arg-saturated nNOSoxy (20 μM) was reduced with dithionite to the levels indicated and then exposed to air. NOHA and citrulline formed in the reactions are shown. Each bar represents the mean ± SD of two independent experiments, each assayed in triplicate.

$Fe^{II}O_2$ complexes of thiol-ligated heme proteins (discussed in refs *18*−*21*), the $Fe^{II}O_2$ complexes of some thiol-ligated heme proteins such as cytochrome P450SCC (substrate-bound) or chloroperoxidase have red-shifted Soret peaks at 423 and 430 nm, respectively (*31*, *32*). For nNOS, the reported differences in Soret position may be due to the different temperatures and solvent conditions [aqueous buffer used here and by Sato et al. (*20*), versus 50% ethylene glycol by Bec et al. (*19*) and Ledbetter et al. (*21*)]. Also, recent crystal structures of inducible NOS and endothelial NOS oxygenase domains all indicate that NOSs have a unique heme environment relative to cytochrome P450 heme proteins (*7*−*9*, *17*, *33*), and our related work suggests that their novel heme environment may be the basis for their red shift in $Fe^{II}O_2$ Soret absorbance.[3] In any case, our current work clearly establishes that the 427 nm $Fe^{II}O_2$ species is both kinetically and chemically competent regarding NO synthesis from NOHA in a single-turnover setting at 10 °C.

Conversion of Arg to NOHA, Citrulline, and Nitrite under Single-Turnover Conditions. We also examined whether the nNOSoxy $Fe^{II}O_2$ species would catalyze product formation from Arg in the single-turnover setting. Experiments that contained Arg instead of NOHA were run as described above and the concentrations of NOHA, citrulline, and nitrite produced in the single-turnover reaction were determined. As shown in Figure 6, when 20 μM nNOSoxy was reduced with dithionite to the level of 1 electron equiv/mol of heme, 3.6 μM NOHA and 1 μM citrulline were formed. When the amount of dithionite was increased to 3 electron equiv/mol of heme, 6.2 μM NOHA and 2.2 μM citrulline were produced. No detectable nitrite was formed from Arg in any case (not shown). The amounts of NOHA and citrulline detected were not increased if the protein was acid-denatured prior to filtration for amino acid analysis, indicating additional products did not remain bound. Inclusion of superoxide dismutase and catalase in the reaction did not diminish the amount of NOHA and citrulline produced. As controls, oxidized enzyme without dithionite did not produce NOHA or citrulline from Arg, and Arg was not converted to products in the absence of enzyme (data not shown).

The fact that some NOHA and citrulline formed from Arg in our single-turnover system implies that some $Fe^{II}O_2$ nNOSoxy molecules received a second electron and converted to an FeO species during the reaction in order to hydroxylate Arg. However, our stoichiometry results suggest that only 20−25% of the nNOSoxy $Fe^{II}O_2$ molecules (percentage calculated on the basis of NOHA + citrulline produced from Arg) were reduced by a second electron. There are five possible sources for the second electron: bound H_4B, excess dithionite, DTT, enzyme-generated superoxide, and a disproportionation reaction between two nNOSoxy molecules.

Bound H_4B could conceivably provide an electron to the $Fe^{II}O_2$ species and convert to the H_3B radical, as previously proposed (*19*). Indeed, an electron provided by H_4B during Arg hydroxylation could help explain why only fully reduced pteridines can support NO synthesis. Recent evidence indicates that bound H_4B can form a radical under single-turnover conditions (*35*). However, if reduction of the $Fe^{II}O_2$ complex by H_4B is a normal feature of Arg hydroxylation, then each bound H_4B should provide one electron to each $Fe^{II}O_2$ molecule, enabling generation of 1 NOHA/heme in the single-turnover reaction. The fact that this stoichiometry has not been achieved in single-turnover experiments by us or by others (*19*) suggests that reduction of the $Fe^{II}O_2$ complex either is highly variable or is uncoupled relative to subsequent formation of the FeO species and its reaction with Arg.

DTT and excess dithionite are unlikely sources of a second electron for the $Fe^{II}O_2$ complex, because DTT cannot enter the active site when Arg or H_4B is bound, and product yield only slightly increased when excess dithionite was intentionally added. Superoxide released during decay of some $Fe^{II}O_2$ complex could also provide an electron to a neighboring $Fe^{II}O_2$ species. However, added SOD did not inhibit product formation. Finally, a disproportionation reaction involving electron transfer between two nNOSoxy molecules after they had bound O_2 can be considered. This would generate a subpopulation of FeO and ferric nNOSoxy molecules, and thus should enable some NOHA formation from Arg, up to a maximum of 0.5 NOHA formed/heme. However, if disproportionation indeed happens in the single-turnover system, it is unclear why product formation from Arg still depends on the presence of H_4B (*19*).

Spectroscopy and Kinetics of Ferrous nNOSoxy Reaction with Oxygen and Arg. We carried out a spectral kinetic study of $Fe^{II}O_2$ formation when the enzyme contained Arg as substrate. A solution of dithionite-reduced nNOSoxy saturated with H_4B and Arg was rapidly mixed with air-saturated buffer at 10 °C. Ninety-six spectra were collected within 0.286 s, 24 of which are shown in Figure 7A. The rapid scan data were best fit to a reaction model A to B to C by the Specfit program, and the calculated spectra for species A−C are shown in Figure 7B. The spectra for species A and C indicate that they are the beginning ferrous and ending ferric nNOSoxy species, respectively. Species B has absorbance maxima at 427 and 557 nm, essentially identical to

[3] S. Adak and D. J. Stuehr, unpublished results.

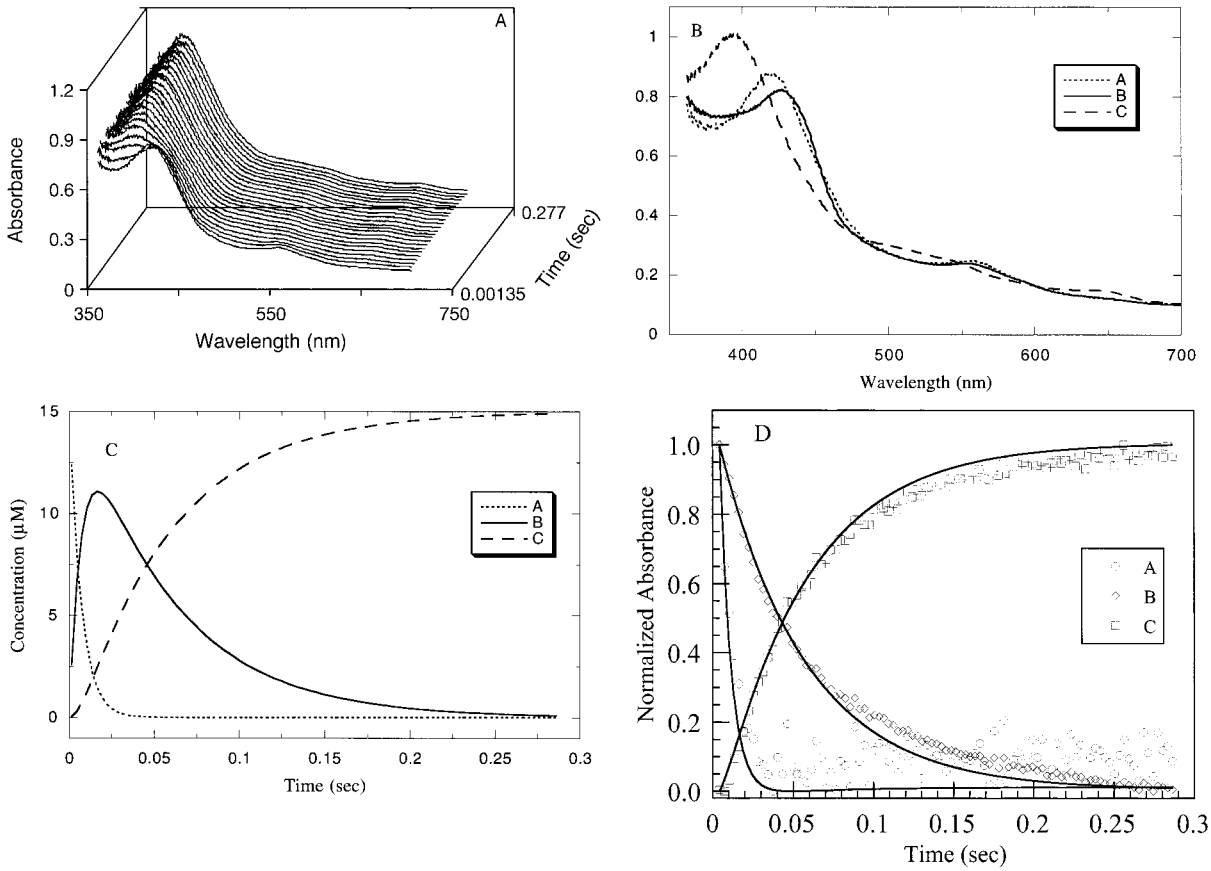

FIGURE 7: Rapid-scan stopped-flow analysis of the reaction of ferrous nNOSoxy with O_2 and Arg. Ferrous nNOSoxy (30 μM) saturated with H_4B and Arg was rapidly mixed with air-saturated buffer at 10 °C. Panel A shows 24 of the 96 consecutive spectra recorded within the first 0.429 s. Panel B shows the Specfit calculated spectra of three distinct species observed during the reaction. Species A, B, and C are the ferrous, $Fe^{II}O_2$, and ferric nNOSoxy, respectively. Panel C contains calculated plots of concentration of species A, B, and C versus time. Panel D compares normalized absorbance values versus time for each species obtained from the data (symbols) with simulated absorbance versus time curves calculated using the kinetic model (—). Representative wavelengths were chosen at or near the absorbance maximum of each species.

the $Fe^{II}O_2$ species that formed in the presence of NOHA. The time course of spectral transitions for seven independent experiments were fit to the sum of two exponentials, giving rate constants of 146 ± 18 and 20 ± 2 s^{-1} for formation and decay of the $Fe^{II}O_2$ species, respectively. The calculated variation in concentrations of ferrous, $Fe^{II}O_2$, and ferric nNOSoxy species during the reaction is shown in Figure 7C, while Figure 7D compares the actual change in absorbance attributed to each species with its simulated change in absorbance. A replica experiment that followed spectral transitions in a reaction between oxygen and an H_4B-saturated ferrous nNOSoxy without substrate gave essentially identical results as when Arg was present (data not shown).

Comparison of actual spectra collected during conversion of the $Fe^{II}O_2$ species to ferric nNOSoxy in the presence of Arg showed that a relatively smooth Soret transition occurs with several isosbestic points appearing in the overlapped traces (Figure 8). This indicates that no spectrally distinct heme−oxy species or NO complex built up during the transition. Because $Fe^{III}OOH$ and FeO complexes of thiol-ligated heme proteins are expected to have different spectra relative to the $Fe^{II}O_2$ species (*26*, *33*, *34*), our spectral data do not provide evidence for further reduction of the $Fe^{II}O_2$ complex in the presence of Arg. Thus, our work suggests that most of the $Fe^{II}O_2$ species was unable to react with Arg during its transition to ferric enzyme:

Scheme 2

$$Fe^{II} \xrightarrow{146\ s^{-1}} Fe^{II}O_2 \xrightarrow{20\ s^{-1}} Fe^{III}$$

Whether bound H_4B provides a second electron to activate the $Fe^{II}O_2$ species remains an important question. Some bound H_4B appears to be oxidized during NO synthesis by NOS (*36*). H_4B also increases the rate of $Fe^{II}O_2$ complex decay (*18*), can form a radical in NOS after $Fe^{II}O_2$ complex formation (*35*), and may increase the proportion of O_2 that is reduced to H_2O_2 during uncoupled NADPH oxidation (*37*). These all suggest that H_4B can give an electron to NOS under certain settings. Our single-turnover results are valuable in this context because they help indicate the degree to which H_4B can provide an electron for Arg hydroxylation. If one assumes that all NOHA and citrulline formed from Arg in our stoichiometry study was coupled to oxidation of bound H_4B, then only 20−25% of bound H_4B gave an electron to the $Fe^{II}O_2$ complex. This is consistent with our spectral evidence during the reaction and suggests that the NOS reductase domain can be a source of the second electron during Arg hydroxylation. Single-turnover and spectral kinetic methods provide a foundation to investigate this and determine what role H_4B plays in both steps of NO synthesis.

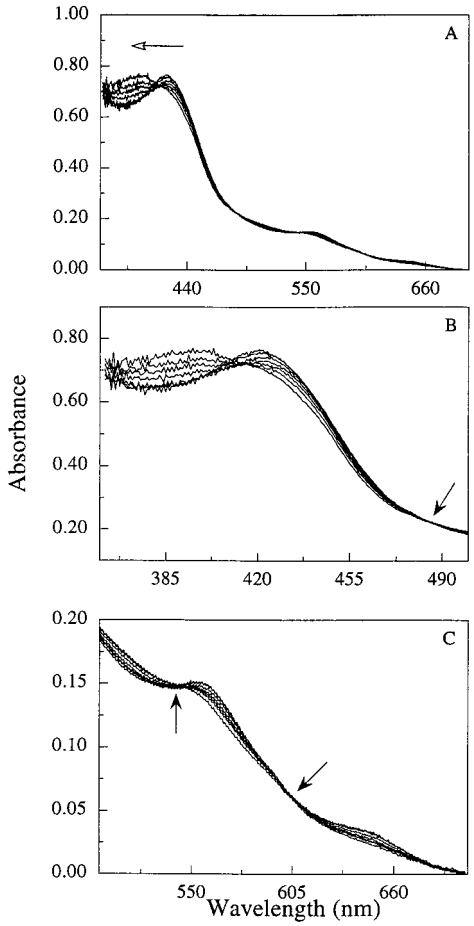

FIGURE 8: Overlay of spectral traces collected during conversion of the Arg-saturated $Fe^{II}O_2$ complex to the ferric nNOSoxy. The seven spectra shown were recorded within the time period of 7.3−40.3 ms. The open arrow shows the direction of Soret spectral shift with time, and the solid arrows indicate isosbestic points. (A) Wavelength range from 360 to 700 nm; (B) expanded region 360−500 nm; (C) expanded region 500−700 nm.

ACKNOWLEDGMENT

We thank Pam Clark for protein expression and purification and Drs. Husam Abu-Soud, Sanjay Ghosh, and Subrata Adak for helpful discussions.

REFERENCES

1. Griffith, O. W., and Stuehr, D. J. (1995) *Annu. Rev. Physiol. 57*, 707−736.
2. Marletta, M. A. (1993) *J. Biol. Chem. 268*, 12231−12234.
3. Mansuy, D., and Renaud, J. P. (1995) in *Cytochrome P450: Structure, Mechanism, and Biochemistry* (Ortiz de Montellano, P. R., Ed.) 2nd ed., pp 537−574, Plenum Press, New York.
4. Mayer, B., and Hemmens, B. (1997) *Trends Biochem. Sci. 22*, 477−481.
5. Masters, B. S. S., McMillan, K., Sheta, E. A., Nishimura, J. S., Roman, L. J., and Martasek, P. (1996) *FASEB J. 10*, 552−558.
6. Stuehr, D. J. (1997) *Annu. Rev. Pharmacol. Toxicol. 37*, 339−359.
7. Crane, B. R., Arvai, A. S., Ghosh, D. K., Wu, C., Getzoff, E. D., Stuehr, D. J., and Tainer, J. A. (1998) *Science 279*, 2121−2126.
8. Fischmann, T. O., Hruza, A., Niu, X. D., Fossetta, J. D., Lunn, C. A., Dolphin, E., Prongay, A. J., Reichert, P., Lundell, D. J., Narula, S. K., and Weber, P. C. (1999) *Nat. Struct. Biol. 5*, 602−611.
9. Li, H., Raman, C. S., Glaser, C. B., Blasko, E., Young, T. A., Parkinson, J. F., Whitlow, M., and Poulos, T. L. (1999) *J. Biol. Chem. 274*, 21276−21284.
10. McMillan, K., and Masters, B. S. S. (1995) *Biochemistry 34*, 3686−3693.
11. Chen, P.-F., Tsai, A.-L., Berka, V., and Wu, K. K. (1996) *J. Biol. Chem. 271*, 14631−14635.
12. Gachhui, R., Ghosh, D. K., Wu, C., Parkinson, J., Crane, B. R., and Stuehr, D. J. (1997) *Biochemistry 36*, 5097−5103.
13. Ghosh, S., Wolan, D., Adak, S., Crane, B. R., Kwon, N. S. K., Tainer, J. A., Getzoff, E. D., and Stuehr, D. J. (1999) *J. Biol. Chem. 274* (in press).
14. Ghosh, D. K., Wu, C., Pitters, E., Moloney, M., Werner, E. R., Mayer, B., and Stuehr, D. J. (1997) *Biochemistry 36*, 10609−10619.
15. Salerno, J. C., Martasek, P., Roman, L. J., and Masters, B. S. S. (1996) *Biochemistry 35*, 7626−7630.
16. Wang, J., Stuehr, D. J., and Rousseau, D. L. (1997) *Biochemistry 36*, 4595−4606.
17. Raman, C. S., Li, H., Martasek, P., Kral, V., Masters B. S. S., and Poulos, T. M. (1998) *Cell 95*, 939−950.
18. Abu-Soud, H. M., Gachhui, R., Raushel, F. M., and Stuehr, D. J. (1997) *J. Biol. Chem. 272*, 17349−17353.
19. Bec, N., Gorren, A. C. F., Voelker, C., Mayer, B., and Lange, R. (1998) *J. Biol. Chem. 273*, 13502−13508.
20. Sato, H., Sagami, I., Daff, S., and Shimizu, T. (1998) *Biochem. Biophys. Res. Commun. 253*, 845−849.
21. Ledbetter, A. P., McMillan, K., Roman, L. J., Masters, B. S. S., Dawson, J. H., and Sono, M. (1999) *Biochemistry 38*, 8014−8021.
22. Fukuto, J. M., Stuehr, D. J., Feldman, P. L., Bova, M. P., and Wong, P. (1993) *J. Med. Chem. 36*, 2666−2670.
23. Abu-Soud, H. M., Presta, A., Mayer, B., and Stuehr, D. J. (1997) *Biochemistry 36*, 10811−10816.
24. Wang, J., Rousseau, D. L., Abu-Soud, H. M., and Stuehr, D. J. (1994) *Proc. Natl. Acad. Sci. U.S.A. 91*, 10512−10516.
25. Korth, H. G., Sustmann, R., Thater, C., Butler, A. R., and Ingold, K. U. (1994) *J. Biol. Chem. 269*, 17776−17779.
26. Benson, D. E., Suslick, K. S., and Sligar, S. G. (1997) *Biochemistry 36*, 5104−5107.
27. Abu-Soud, H. M., Wu, C., Ghosh, D. K., and Stuehr, D. J. (1998) *Biochemistry 37*, 3777−3786.
28. Huang, L., Abu-Soud, H. M., Hille, R., and Stuehr, D. J. (1999) *Biochemistry 38*, 1912−1920.
29. Scheele, J. S., Bruner, E., Kharitonov, V. G., Martasek, P., Roman, L. J., Masters, B. S. S., Sharma, V. S., and Magde, D. (1999) *J. Biol. Chem. 274*, 13105−13110.
30. Abu-Soud, H. M., Wang, J., Rousseau, D.L., Fukuto, J., Ignarro, L. J., and Stuehr, D. J. (1994) *J. Biol. Chem. 270*, 22997−23006.
31. Tuckey, R. C., and Kamin, H. (1982) *J. Biol. Chem. 257*, 9309−9314.
32. Sono, M., Eble, K. S., Dawson, J. H., and Hager, L. P. (1985) *J. Biol. Chem. 260*, 15530−15535.
33. Larroque, C., Lange, R., Maurin, L., Bienvenue, A., and van Lier, J. E. (1990) *Arch. Biochem. Biophys. 282*, 198−201.
34. Palcic, M. M., Rutter, R., Araiso, T., Hager, L. P., and Dunford, B. (1980) *Biochem. Biophys. Res. Commun. 94*, 1123−1127.
35. Hurshman, A. R., Krebs, C., Edmondson, D. E., Huynh, B. H., and Marletta, M. A. (1999) *Biochemistry 38*, 15689−15696.
36. Witteveen, C. F. B., Giovanelli, J., and Kaufman, S. (1999) *J. Biol. Chem. 274*, 29755−29762.
37. Vasquez-Vivar, J., Hogg, N., Martasek, P., Karoui, H., Pritchard, K. A., Jr., and Kalyanaraman, B. (1999) *J. Biol. Chem. 274*, 26736−26742.
38. Clague, M. J., Wishnok, J. S., and Marletta, M. A. (1997) *Biochemistry 36*, 14465−14473.

BI9920228